Journal of Quantitative Spectroscopy & Radiative Transfer 230 (2019) 1–12

Contents lists available at ScienceDirect

Journal of Quantitative Spectroscopy & Radiative Transfer

journal homepage: www.elsevier.com/locate/jqsrt

The instrumental line shape of the atmospheric chemistry experiment Fourier transform spectrometer (ACE-FTS)

C.D. Boone [a,*], P.F. Bernath [a,b]

[a] Department of Chemistry, University of Waterloo, 200 University Avenue West, Ontario N2L 3G1, Canada
[b] Department of Chemistry and Biochemistry, Old Dominion University, Norfolk, VA 23529, USA

ARTICLE INFO

Article history:
Received 11 December 2018
Revised 22 March 2019
Accepted 22 March 2019
Available online 23 March 2019

Keywords:
Infrared Fourier transform spectroscopy
Instrumental line shape

ABSTRACT

Accurate modeling of the instrumental line shape (ILS) of a Fourier transform spectrometer (FTS) is crucial for minimizing systematic errors in the analysis of FTS measurements. Isolated spectral features having widths much less than the ILS width can be used to determine a representation for the ILS. The instrument modulation function at a particular wavenumber can be calculated from the Fourier transform of an isolated spectral feature. Accounting for known contributions from the finite field of view and the shape of the spectral feature in the infinite resolution spectrum, one can directly observe the contribution from all additional sources of self-apodization to the instrument modulation function. This simplifies determination of the appropriate empirical function(s) to best characterize these additional self-apodization effects, alleviating the need to guess at forms for the empirical function. Lines spanning the instrument spectral range are analyzed to determine a wavenumber dependence for the empirical representation. This approach is employed to characterize the ILS for the Atmospheric Chemistry Experiment Fourier transform spectrometer (ACE-FTS), a high resolution (0.02 cm^{-1}) satellite-based instrument used for solar occultation studies of the Earth's atmosphere.

© 2019 Published by Elsevier Ltd.

1. Introduction

Fourier transform spectrometry [1] is a powerful tool for remote sensing of the Earth's atmosphere. The Fourier transform spectrometer (FTS) has a long heritage in the field of remote sensing, including satellite-based missions [2–8], balloon-borne instruments [9,10], and ground-based monitoring networks [11,12]. The FTS also plays a vital role in laboratory studies for molecules of atmospheric interest [e.g., 13,14], helping supply the spectroscopic information required to analyze remote sensing measurements.

Knowledge of the instrumental line shape (ILS) is key to deriving the most accurate possible results from FTS measurements. In the past, it was common practice to apodize FTS measurements [15], a convenient means to suppress the ringing of ILS sidelobes in the spectra. However, increasingly stringent precision and accuracy targets in remote sensing studies [16] have driven an inclination to carefully characterize these sidelobes rather than artificially suppress them with apodization.

1.1. The modulation function

In practice, calculation of the ILS begins with an assumed modulation function (MF), a measure of the modulation efficiency as a function of optical path difference over the course of the interferometer scan. The modulation function can be expressed as follows [17]:

$$MF(\tilde{\nu}, x) = F_{clip} * \eta(\tilde{\nu}, x) * \frac{\sin\left(\frac{1}{2}\pi r^2 \tilde{\nu} x\right)}{\frac{1}{2}\pi r^2 \tilde{\nu} x}, \tag{1}$$

where x is optical path difference in cm, $\tilde{\nu}$ is wavenumber (cm^{-1}), and r is one-half of the angular diameter of the instrument's circular input aperture.

The term F_{clip} is a rectangular windowing function that represents the finite scan length of the instrument. Shown in Fig. 1 for the case of a double-sided interferometer, the function has a value of 1 for optical path differences between ± maximum optical path difference (MOPD) and a value of 0 otherwise. The ILS arising from this ideal, lossless modulation function would be a pure sinc (i.e., sinx/x) function. However, changes in modulation efficiency as a function of optical path difference for real instruments yield deviations from this ideal case.

The third term on the right-hand side in Eq. (1) accounts for a form of self-apodization arising from off-axis rays in the

* Corresponding author.
E-mail address: cboone@scisat.ca (C.D. Boone).

https://doi.org/10.1016/j.jqsrt.2019.03.018
0022-4073/© 2019 Published by Elsevier Ltd.

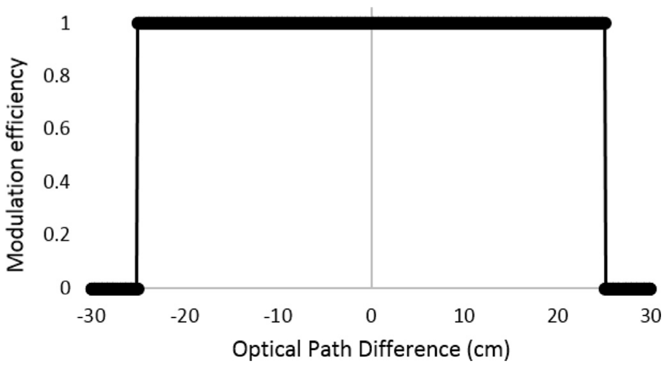

Fig. 1. Ideal modulation function for a double-sided Fourier transform interferometer with a maximum optical path difference of 25 cm.

instrument, the so-called field-of-view effect [1]. This term is a sinc function of optical path difference, x, and varies with wavenumber, exhibiting increasing self-apodization with increasing wavenumber.

The second term on the right-hand side in Eq. (1), $\eta(\tilde{\nu},x)$, represents self-apodization from all other factors that impact the variation of modulation efficiency with optical path difference, for example FTS mirror misalignment [18]. The imaginary component of this complex function characterizes phase effects in the instrument that give rise to asymmetry in the ILS.

The form of $\eta(\tilde{\nu},x)$ can be determined from the analysis of spectral features having widths much less than the ILS width. The function will vary with wavenumber, and so the analysis should be performed for a collection of spectral features at different wavenumbers, ideally spanning the entire wavenumber range of interest for the instrument. If the variation with wavenumber is reasonably smooth, one can determine $\eta(\tilde{\nu},x)$ at a discrete set of wavenumbers and interpolate between. Alternatively, one can use a set of empirical functions to reproduce the modulation function and determine variations with wavenumber for parameters in the empirical functions. The latter approach will be used in this study.

1.2. The atmospheric chemistry experiment

Developed under the auspices of the Canadian Space Agency, the Atmospheric Chemistry Experiment is a satellite-based mission for remote sensing of the Earth's atmosphere [6,19]. On board the small science satellite SCISAT, it was launched August 12, 2003 into a circular, highly inclined orbit (650 km altitude, 74° inclination). The measurement technique employed is solar occultation. Using the sun as a light source, the instruments collect a series of atmospheric measurements as the sun rises or sets from the orbiting satellite's perspective, providing up to 30 measurement opportunities per day.

The primary instrument on SCISAT is the Atmospheric Chemistry Experiment Fourier transform spectrometer (ACE-FTS), a fully tilt and shear compensated FTS with high resolution (±25 cm maximum optical path difference, 0.02 cm^{-1} resolution) and broad spectral coverage in the mid infrared (750 to 4400 cm^{-1}), featuring a signal-to-noise ratio ranging from just under 100:1 up to ~400:1 [20]. It uses a multi-pass design to generate high resolution from a compact instrument. The scan mechanism consists of cube corner retroreflectors mounted on a rotary scan double pendulum, similar to the MB100 instrument developed by ABB (formerly known as Bomem), the ACE-FTS instrument primary contractor. The instrument circular input aperture has an angular diameter of 1.25 mrad. A factor of 5 magnification is applied within the instrument, which yields an "internal field of view" diameter of 6.25 mrad.

ACE-FTS measurements have been used to determine altitude profiles for atmospheric pressure, temperature, and the volume mixing ratios of dozens of molecules with spectral features in the infrared [17,19,21]. Information on aerosols can also be derived from ACE-FTS spectra, such as polar stratospheric clouds [22], polar mesospheric clouds [23], and volcanic plumes [24].

2. The ACE-FTS modulation function amplitude

There exists a software package called LINEFIT [18] that is routinely employed to determine the ILS of ground-based FTS instruments. The "extended parameter set" option of the software performs a constrained fit for 20 optical path difference points in both amplitude and phase of the modulation function (a total of 40 coupled parameters). However, there were indications of structure in the ACE-FTS modulation function near maximum optical path difference, related in some fashion to the instrument design rather than optical effects, which could pose challenges for analysis with this software package.

Fortunately, with adequate knowledge of the line shape of an isolated spectral feature, it is possible to directly calculate the instrument modulation function. There is no need to guess at the form of an empirical function to use for $\eta(\tilde{\nu},x)$ from Eq. (1), as was done when generating the ILS for version 3 processing of ACE-FTS data [17]. Both the amplitude and phase of the modulation function can be directly observed with no assumptions required beyond the shape of the spectral feature in the infinite resolution spectrum.

Uncertainties can be minimized by employing low pressure measurements. If the lines are close to Doppler-limited, the shape will have minimal sensitivity to pressure and relatively low sensitivity to temperature, since the Doppler width varies as the square root of temperature. At low pressures, other line shape effects such as speed dependence and line mixing will be negligible and therefore do not complicate the analysis. High altitude ACE-FTS solar occultation measurements, with pressures ranging from 0.01 to 1×10^{-8} atm, were employed in this analysis.

Calculating a spectrum to employ in the analysis of FTS measurements involves the convolution of a calculated infinite resolution spectrum with the FTS ILS. Conversely, taking the Fourier transform of an isolated line from an FTS measurement yields the modulation function (the Fourier transform of the ILS) at the given wavenumber multiplied by the Fourier transform of the infinite resolution spectral feature, since convolution in wavenumber space equates to multiplication in the Fourier (optical path difference) space. Thus, the amplitude (i.e., the real component) of the modulation function can be directly calculated by taking the Fourier transform of an isolated line from an FTS measurement and dividing through by the Fourier transform of the calculated line in the infinite resolution spectrum.

A previous study [25] employed the identical approach used here for removing the contribution from the spectrum in the modified modulation function: dividing out the Fourier transform of the calculated infinite resolution spectrum. However, that study makes no mention of how they accounted for the field of view effect in the analysis. They also did not address the wavenumber dependence of the instrumental line shape, generating a single ILS curve from a small set of HBr lines. They also applied a weighting function that removed any sensitivity to the far wing of the ILS. No such weighting function was required in the current analysis, but note that the ACE-FTS has lower resolution, and we averaged thousands of spectra to reduce noise effects, which represents close to ideal conditions for the analysis approach described here.

Other studies [e.g., 26,27] exploited the information inherent in the Fourier transform of the measured signal, but their approach involved subtracting a fitted curve of the form

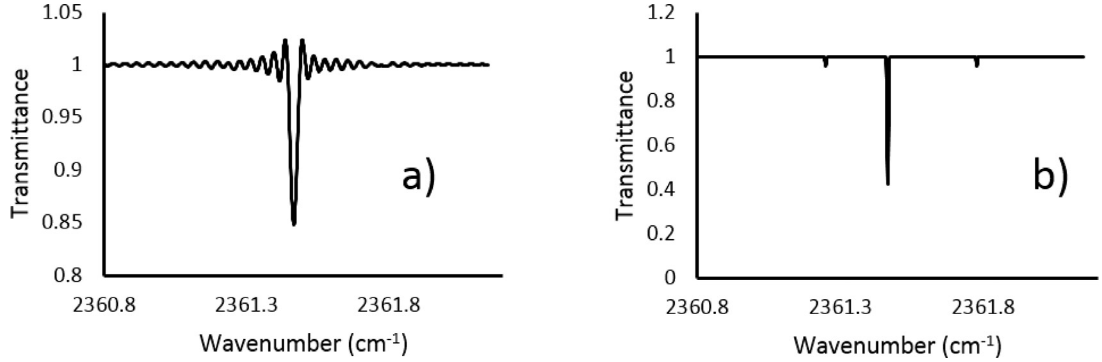

Fig. 2. (a) The averaged transmittance spectrum for a relatively isolated CO_2 line from >6000 ACE-FTS high altitude measurements. (b) The averaged calculated infinite resolution spectrum corresponding to the same set of 6000+ measurements.

exp(-ax – bx^2) (where x is optical path difference and a and b are empirical parameters) from the modulation function amplitude. This was a means to remove the contribution from the line shape in the infinite resolution spectrum as well as an approximate form for the field of view effect. However, this would also remove contributions from instrumental effects beyond the field of view effect that exhibit similar variation with optical path difference. The current study retains all instrumental contributions to the modulation function at the expense of relying strongly on knowledge of the line shape in the infinite resolution spectrum.

In the absence of asymmetry in the line itself, the phase of the modulation function is simply the imaginary component of the Fourier transform of an isolated line in the FTS measurement, with no adjustments for contributions from the spectrum required (unlike the amplitude), as will be discussed in Section 3.

2.1. Residual modulation function

Fig. 2a shows an averaged CO_2 line from a set of high altitude ACE-FTS transmittance measurements. The averaging was done for spectra with tangent heights between 105 and 130 km. The wavenumber calibration of ACE-FTS spectra varies with ambient temperature on the satellite, and so each measured line was aligned with a calculated spectrum (using wavenumber shifts derived from cross-correlation of the measured and calculated spectra) before inclusion in the average. Only lines with peak transmittance less than 0.95 in the FTS spectrum were included in the average, to ensure a sufficiently strong signal for noise to have a negligible impact on the alignment with the calculated spectrum. Only those lines with peak transmittance greater than 0.1 in the calculated infinite resolution spectrum were included in the average, to avoid saturation effects. The average calculated infinite resolution spectrum is shown in Fig. 2b, where the calculated spectra were based on previously generated retrieval results for the occultations. More than 6000 spectra from ~2800 occultations went into the averages shown in Fig. 2. The data from the ACE-FTS are minimally sampled, with a spacing of 0.02 cm^{-1}. The measurement in Fig. 2a (and subsequent figures) has been Fourier interpolated by a factor of 16 to better see details.

The cross-correlation alignment of the measured spectrum employed narrow windows (containing only the isolated line) on the interpolated wavenumber grid with spacing 0.02/16 cm^{-1}. The instrument's high signal-to-noise ratio ensures alignment to a small fraction of this wavenumber spacing, and a strong filter on the average to remove outliers minimizes apparent broadening of the line from averaging slightly misaligned spectra. However, one cannot ensure perfect alignment of every spectrum, which represents a systematic error in the analysis.

Note the presence of two weaker CO_2 lines in the spectral window, clearly visible in Fig. 2b. The intent here was to find an isolated line from which we could calculate the modulation function via the Fourier transform of the measurement, and these weak interferers complicate matters. In atmospheric spectra, it is difficult to find completely isolated lines. However, if the "interfering" lines are weak compared to the main spectral feature in the window, it is possible to calibrate out the weak lines. This is accomplished by dividing out a scaled and shifted version of the measured spectrum for each weak interfering line: i.e., shifting to align the main spectral feature with the weak feature and scaling such that dividing through removes the contribution of the weak line. In this process, it is important to avoid having secondary features that are too strong relative to the primary spectral feature.

In the current study, information on the shifts required to align the main spectral feature with the secondary features was derived from the calculated infinite resolution spectrum. However, the relative intensities of the weak CO_2 lines in the calculated spectrum were not reliable, because the lines were impacted by non-local thermodynamic equilibrium effects at these high altitudes [28]. Thus, scaling factors in the calibration process were determined "by hand," tuned to generate minimum residuals in the final analysis results.

Fig. 3a shows the adjusted FTS spectrum with the weak secondary features calibrated out, the baseline removed (via subtracting off a constant roughly equal to 1.0), and a normalization applied (such that the integral = 1). Note that the normalization serves to flip this transmittance spectrum to positive-pointing, making it resemble an absorbance. If the line is not sampled at the peak, an artificial phase error will be introduced into the imaginary component of the Fourier transform, a phase error that varies linearly with optical path difference. Therefore, the line in Fig. 3a has been resampled such that one of the data points is at the line's peak. Fig. 3b shows the adjusted calculated infinite resolution spectrum, with the secondary peaks zeroed out, the baseline subtracted, and a normalization applied. This curve was not resampled to capture the peak because the calculated line shape is symmetric by design, and the imaginary component of its Fourier transform is therefore of no consequence.

Note that the x-axis is zoomed by a factor of ~5 in Fig. 3b relative to Fig. 3a in order to better see the small width of the line in the calculated infinite resolution spectrum, much narrower than the ILS.

There is asymmetry in the measured line (Fig. 3a, with a zoom of the y-axis provided in Fig. 3c to better see details of the sidelobes) that was not accounted for in previous ACE-FTS processing versions. There is asymmetry near line center, as evinced by differences in the depths of the first minima on either side of line center in Fig. 3c. Looking closely at the sidelobes, there

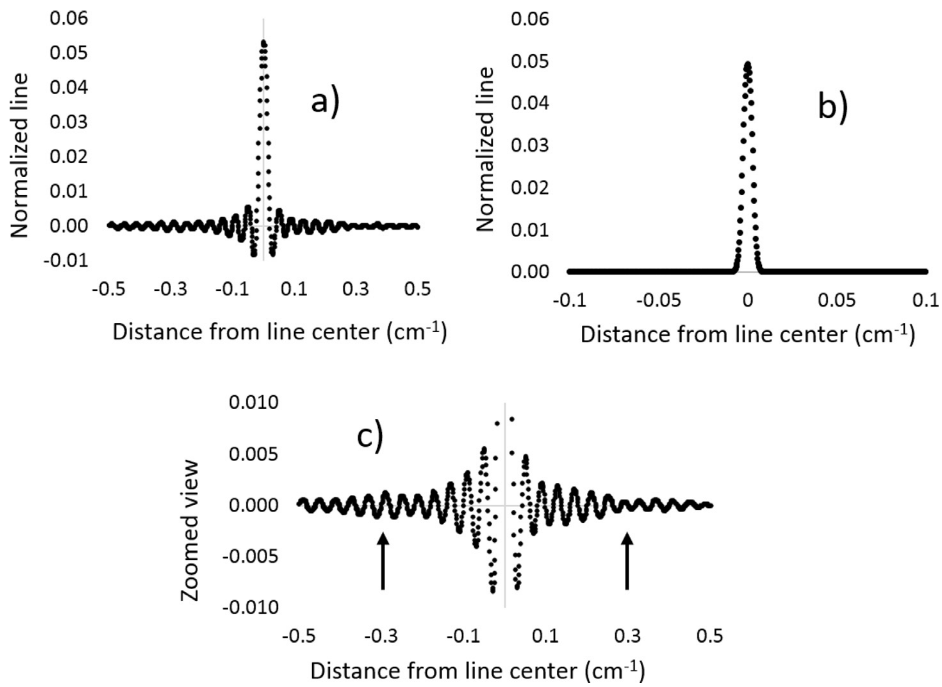

Fig. 3. (a) The measurement from Fig. 2a with weak interfering lines calibrated out, the baseline removed, a normalization applied, and a resampling to capture the line's peak. (b) The calculated infinite resolution spectrum from Fig. 2b with the contributions from weak interfering lines zeroed out, the baseline removed, and a normalization applied. (c) A zoom on the y-axis of Fig. 3a. Arrows indicate regions of sidelobe amplitude enhancement (on the left) and suppression (on the right).

exists an additional asymmetry from a periodic pattern of amplitude enhancement and reduction: wherever there is an enhancement in sidelobe amplitude located some distance from line center (for example, the location indicated by the arrow on the left in Fig. 3c), there is a reduction in amplitude the same distance on the opposite side of line center (as indicated by the arrow on the right in Fig. 3c). The consequences of these asymmetries on the phase of the modulation function will be explored in Section 3.

Proper treatment of the baseline in the average spectrum is important when generating the curve in Fig. 3a. Subtracting the baseline reduces edge effects when taking the Fourier transform. Baseline removal for these high-altitude ACE-FTS measurements involves subtracting a constant value (the baseline level in the transmittance measurement) from each data point. Ideally, this baseline level would be exactly 1.0, but in practice there was generally a small offset from that value, typically less than 0.001. If the baseline of the adjusted FTS line in Fig. 3a is not at zero, there will be a sinc function superimposed on its Fourier transform, from the apparent pedestal under the line. In the current study, baseline subtraction was fine-tuned by hand for some lines in order to remove indications of a superimposed sinc function.

Care should be taken if the spectra to be analyzed feature significant channeling. Large variations in the baseline in a small spectral window from channeling will introduce effective noise in the Fourier transform, thereby complicating the analysis. The effect can be removed by characterizing the channeling (e.g., by fitting to a sinusoidal function) and dividing it out. In the current study, regions exhibiting channeling or incompletely canceled solar features in the transmittances were excluded from the analysis.

Taking the real component of the Fourier transform of the isolated spectral feature in Fig. 3a yields the curve shown in Fig. 4 labeled "Modified modulation function." Also shown in Fig. 4 is the Fourier transform of the adjusted infinite resolution spectrum from Fig. 3b. It is labeled as "Line apodization" because the process of convolving an infinite resolution spectrum with the FTS ILS serves as an effective apodization, the reason sidelobes are suppressed in FTS measurements when the widths of lines in the infinite resolution spectrum approach or surpass the ILS width. This effective apodization arises from the spectrum, not the instrument, and therefore the effect must be removed in order to determine the modulation efficiency curve associated with the instrument itself. Fortunately, removing the effect is simple, a point by point division of the "Modified modulation function" curve by the "Line apodization" curve in Fig. 4, which yields the true modulation function for the instrument at the given wavenumber (not shown).

The self-apodization curve resulting from the finite field of view effect (labeled "FOV effect") is also shown in Fig. 4. This was calculated from the sinc term in Eq. (1), using the assumed 6.25 mrad diameter internal field of view ($r = 0.003125$ rad) and the wavenumber of the line ($\tilde{\nu} = 2361$ cm^{-1}). Dividing the true modulation function (i.e., the modified modulation function divided by the line apodization) by the known FOV effect contribution yields what we will refer to as the "residual modulation function", which we shall characterize with an empirical function.

The residual modulation function will vary as a function of wavenumber. Therefore, a set of isolated lines spanning as much of the instrument wavenumber range as possible was selected. Table 1 shows the positions of these lines, as well as the altitude range searched for lines matching the criteria described earlier (measured peak transmittance less than 0.95, calculated infinite resolution spectrum peak greater than 0.1) to include in the average. The width of the spectral window varied from line to line, typically between 1.2 and 2 cm^{-1}, carefully chosen to avoid strong interfering lines and excessive far wing sidelobes from neighboring lines.

For each line listed in Table 1, residual modulation functions were generated. The first step in this process consisted of collecting averages for the lines from ACE-FTS spectra as well as averages for the associated calculated infinite resolution spectra. Contributions from weak interfering lines were removed from the averaged ACE-FTS spectra to yield isolated spectral features, and baselines were removed to avoid edge effects, as described previously.

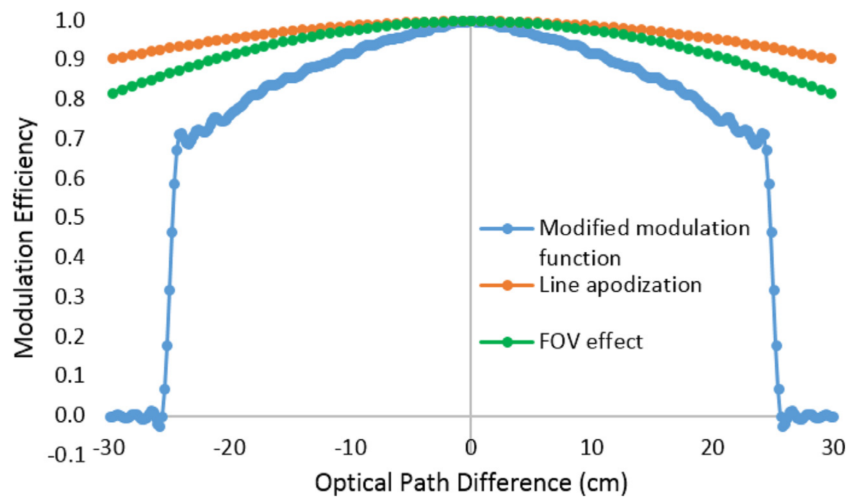

Fig. 4. In blue: the modified modulation function amplitude, the real component of the Fourier transform of the curve in Fig. 3a. In orange: the real component of the Fourier transform of the curve in Fig. 3b, a contribution to the modified modulation function that arises from the spectrum and not the instrument itself. In green: the field of view effect arising from off-axis rays in the interferometer. All are expressed as a factor relative to the modulation efficiency at zero path difference.

Table 1
Isolated lines employed in the determination of the ACE-FTS ILS.

Line (cm^{-1})	Molecule	Altitude range (km)	Line (cm^{-1})	Molecule	Altitude range (km)
945.98	CO_2	35–55	3064.40	H_2O	50–70
1311.43	CH_4	45–75	3133.07	H_2O	50–72
1404.99	H_2O	47–80	3178.12	H_2O	50–75
1487.35	H_2O	55–87	3254.15	H_2O	47–70
1554.35	H_2O	60–87	3291.36	H_2O	40–60
1627.83	H_2O	62–90	3334.63	H_2O	35–57
1739.84	H_2O	62–90	3385.71	H_2O	40–65
1756.82	H_2O	58–82	3420.50	H_2O	50–67
1792.66	H_2O	62–88	3540.33	CO_2	65–80
1869.35	H_2O	58–82	3592.61	CO_2	85–100
2099.08	CO	70–115	3616.66	CO_2	85–102
2139.43	CO	70–110	3694.32	CO_2	85–102
2183.22	CO	70–115	3759.84	H_2O	70–86
2272.00	$^{13}CO_2$	85–105	3807.01	H_2O	75–90
2337.66	CO_2	100–130	3891.30	H_2O	70–85
2361.47	CO_2	105–130	3953.10	H_2O	53–70
2366.65	CO_2	100–130	4008.57	H_2O	45–65
2416.06	CO_2	30–50	4038.96	HF	38–55
2540.36	N_2O	30–45	4088.13	H_2O	35–55
2944.91	HCl	40–55			

Modified modulation functions were calculated by taking the Fourier transform of the resulting curves. True modulation functions were calculated by dividing through by the Fourier transform of the calculated infinite resolution spectra (the “line apodization” described previously). The residual modulation functions were then calculated by dividing through by the known contributions from the field of view effect at the given wavenumbers.

2.2. The empirical function

With the set of residual modulation functions spanning the ACE-FTS measurement range in hand, the task becomes selecting an empirical function or set of functions that accurately reproduces the observations, ideally with a minimal number of parameters.

Looking at Fig. 4, the ACE-FTS modulation function does not exhibit an abrupt switch off in modulation efficiency at MOPD, as one might expect given the windowing function shown in Fig. 1. Instead, the drop off begins at a smaller optical path difference, falling rapidly to zero at MOPD. This verifies the observation from the ILS determination for version 3 processing [17] that a steep decline (rather than a sharp cut off) near MOPD significantly improved fitting residuals. The reason for the behavior is not clear, perhaps associated with a slowing down of the scanning mechanism for turnaround.

Note that, working with windows of a finite wavenumber extent, one would not expect the ideal windowing function in Fig. 1. Rather, one would obtain a “smearing” of the edges, such that the points at +/− MOPD were at roughly half the expected value, accompanied by ringing in the vicinity of the edge. The observed phenomenon near MOPD spans several points, well beyond the effect such a smearing artifact could impart in the calculated Fourier transform.

The nature of this feature near MOPD does not appear to vary significantly with wavenumber, and so accounting for it requires only two parameters: the optical path difference at which the rapid drop off begins (denoted as the “cliff edge”) and the linear rate of decline in modulation efficiency between that point and MOPD (denoted “cliff slope”).

In addition to the steep drop off near MOPD, there is a component in the residual modulation function that increases nonlinearly with increasing optical path difference, similar to the “line apodization” and “FOV effect” curves in Fig. 4. A common practice in the analysis of FTS spectra is to compensate for ILS deficiencies by using an effective value for the field of view diameter, treating it as an empirical parameter [e.g., 29,30]. The ILS generated for ACE-FTS version 3 processing [17] employed this strategy, accounting for the larger than expected line width by inflating the field of view, with a different value used for the two detector regions of the instrument. This approach has the benefit of a built-in variation with wavenumber from a single parameter, potentially reducing the complexity required in the empirical modeling.

However, it turned out that a Gaussian line shape reproduced the residual modulation function significantly better than increasing the effective field of view did, dramatically improving the fitting quality. The implication is that the general practice of mitigating ILS problems by adjusting the field of view may need to be re-evaluated, at least for situations where the effective field of view differs significantly from the physical one. Note that the origin of this Gaussian self-apodization acting on the ACE-FTS modulation function is unknown. If this approach is to be applied to other instruments, it is unclear if one should expect the same shape from the self-apodization sources (i.e., sources beyond the line apodization and the field of view effect) specific to that instrument. One should always examine the calculated residual modulation functions to verify the appropriate shape.

The shape of the Gaussian apodization function varies according to:

$$e^{-\frac{1}{2}\left(\frac{x}{a_G(\tilde{\nu})}\right)^2}, \tag{2}$$

where x is optical path difference in cm and $a_G(\tilde{\nu})$ describes the width of the Gaussian apodization function at wavenumber $\tilde{\nu}$. For the wavenumber dependence, a cubic variation was found to provide sufficient accuracy:

$$a_G(\tilde{\nu}) = a_{G0} + a_{G1} * (\tilde{\nu} - 2400) + a_{G2} * (\tilde{\nu} - 2400)^2 + a_{G3} * (\tilde{\nu} - 2400)^3, \tag{3}$$

where 2400 is a wavenumber near the center of the ACE-FTS range. Note that different forms for the wavenumber variation were explored before settling on a form that yielded a combination of small fitting residuals and statistical errors on all fitted parameters that were smaller than the values of the parameters.

Thus, the residual modulation function amplitude (which equates to $F_{clip} * \eta(\tilde{\nu}, x)$ from Eq. (1)) can be represented accurately across the entire ACE-FTS wavenumber range by a set of six parameters: the two parameters describing the behavior near MOPD (cliff edge and cliff slope), plus the four parameters in Eq. (3) (a_{G0}, a_{G1}, a_{G2}, and a_{G3}).

3. The ACE-FTS modulation function phase

In the absence of line asymmetry in the infinite resolution spectrum, the modulation function phase is simply the imaginary component of the Fourier transform of an isolated FTS line (e.g., the Fourier transform of the curve in Fig. 3a). Fig. 5a shows the average phase for lines in the 1300 to 1800 cm^{-1} range. Note that for individual lines there are generally spikes in the calculated phase at MOPD, likely a consequence of far-wing sidelobes from neighboring lines "polluting" the spectral window. These spikes exhibit high variability from line to line but effectively average out for the curve in Fig. 5a. At lower wavenumber, there is relatively low variability in the phase other than the spikes at MOPD.

There is significant structure in the curves in Fig. 5 for optical path differences approaching MOPD. The origins of these phase effects are unknown, but this structure must be taken into account to accurately reproduce the ACE-FTS ILS.

Note that, owing to the nature of the convolution process, the ILS is actually the mirror image of the shape observed in the measured spectrum. As such, the phase of the ILS will be the inverse of the curves in Fig. 5 (i.e., they must be multiplied by −1).

At higher wavenumbers, there are additional contributions to the phase that increase with increasing wavenumber. Fig. 5b shows the average phase for lines between 3600 and 4000 cm^{-1}. These contributions to the phase at higher wavenumbers can be modeled reasonably efficiently by two functions (dispersion-type and sine) that are opposite in phase.

3.1. The empirical function

The first component of the empirical representation of the modulation function phase is the curve in Fig. 5a, a "baseline contribution" that was determined from the average observed phase for lines at lower wavenumbers. This is a fixed contribution at all wavenumbers, added directly to every calculated phase. At low wavenumbers, where the phase exhibits little variation, this represents the only significant contribution to the phase. The chosen conditions for ILS calculation may involve a different sampling than the points in Fig. 5a, in which case cubic spline interpolation is used to resample the curve in Fig. 5a onto the required grid.

In addition to the baseline contribution, we have two functions with opposite phase that are used to model the phase at higher wavenumbers. The first of these, a dispersion-type term (which does not follow the standard definition of a dispersion shape, but is perhaps more appropriately classified as the derivative of a Lorentzian shape) is expressed as:

$$\frac{a_D(\tilde{\nu}) * x}{\left(b_D + x^2\right)^2}, \tag{4}$$

where x is optical path difference in cm. The width of the function, defined by the parameter b_D, does not vary with wavenumber, but the coefficient $a_D(\tilde{\nu})$ requires a quadratic variation as a function of wavenumber:

$$a_D(\tilde{\nu}) = a_{D0} + a_{D1} * (\tilde{\nu} - 750) + a_{D2} * (\tilde{\nu} - 750)^2, \tag{5}$$

where 750 is the lower wavenumber limit of the usable ACE-FTS range.

The second function employed to characterize the modulation function phase at higher wavenumbers is defined as follows:

$$a_S(\tilde{\nu}) * \sin(x * b_S), \tag{6}$$

where x is again optical path difference in cm. The parameter b_S is assumed constant as a function of wavenumber, while the coefficient $a_S(\tilde{\nu})$ is assigned a quadratic variation:

$$a_S(\tilde{\nu}) = a_{S0} + a_{S1} * (\tilde{\nu} - 750) + a_{S2} * (\tilde{\nu} - 750)^2. \tag{7}$$

Thus the empirical representation of the modulation function phase consists of a "baseline contribution" (the curve in Fig. 5a), plus the two empirical functions in Eqs. (4) and (6) with a total of 8 parameters (a_{D0}, a_{D1}, a_{D2}, b_D, a_{S0}, a_{S1}, a_{S2}, and b_S), where these parameters are defined in Eqs. (4)–(7). Combining this with the empirical representation of the modulation function amplitude from Section 2, we can now calculate the ACE-FTS ILS at any wavenumber.

4. Fitting averaged spectra

Direct calculation of modulation function amplitude and phase for a number of lines across the ACE-FTS wavenumber range enabled determination of the appropriate empirical representation of the ACE-FTS instrumental line shape, as well as the ideal forms for wavenumber dependences for parameters in this empirical representation. The structure in the ACE-FTS modulation function near MOPD would have made it challenging to achieve comparable accuracy in the ILS characterization in any other fashion.

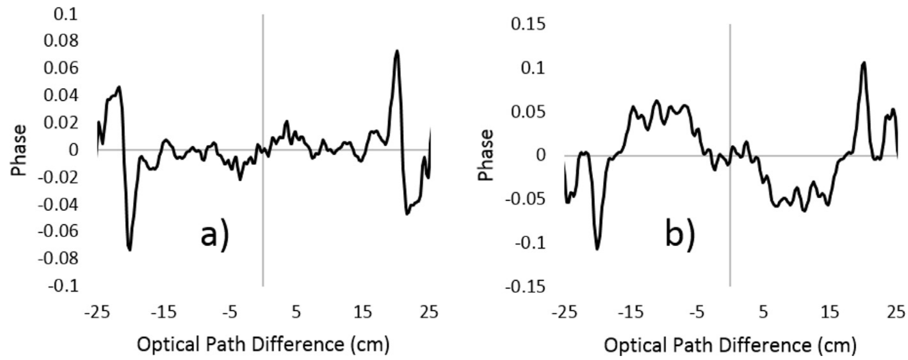

Fig. 5. (a) The average phase for lines between 1300 and 1800 cm^{-1}. (b) The average phase for lines between 3600 and 4000 cm^{-1}.

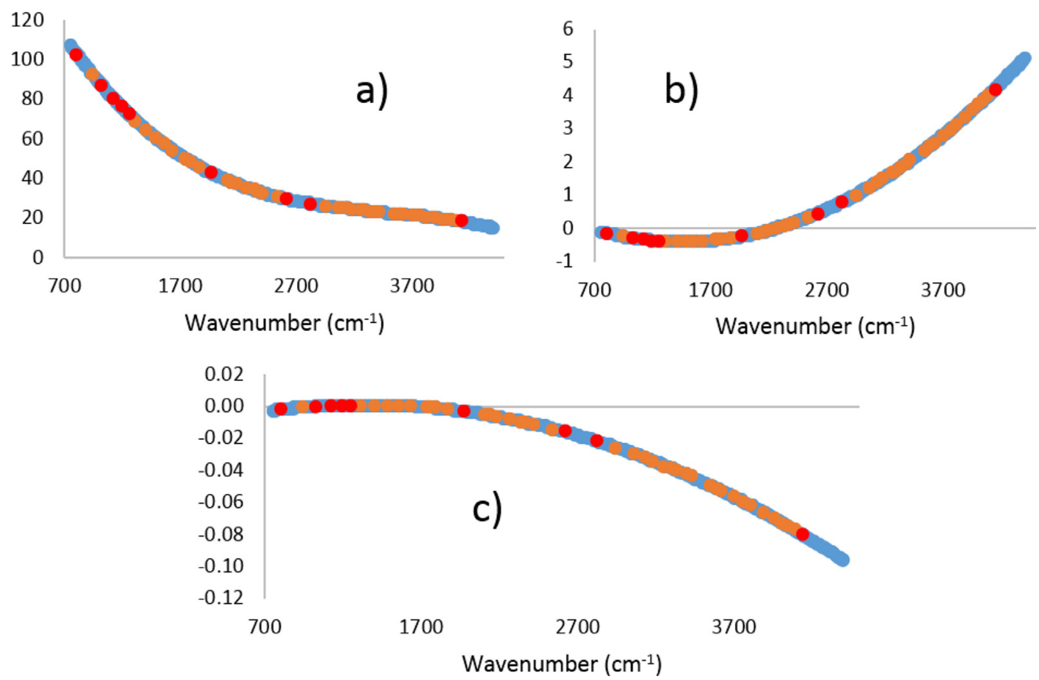

Fig. 6. Wavenumber dependences for the parameters: (a) $a_G(\tilde{\nu})$, (b) $a_D(\tilde{\nu})$, and (c) $a_S(\tilde{\nu})$. Orange points indicate the locations of isolated spectral features employed in the analysis, while red points indicate the locations of multi-line windows.

However, once the empirical representation has been established, it is more appropriate to determine the final values for the empirical parameters from a fitting of the original lines rather than fitting the derived modulation function amplitude and phase. When taking the Fourier transform of real measurements, noise features and effective noise (e.g., channeling, far wing sidelobes from neighboring lines, or weak lines that were not calibrated out) could manifest in unanticipated ways in the calculated modulation function, with information on the symmetric component contained in the real part and information on the asymmetric component gathered in the imaginary part. Fitting the original lines ensures internal consistency between amplitude and phase, by determining the two quantities simultaneously.

Perhaps most importantly, fitting the original lines rather than the derived modulation functions permits the inclusion of additional lines in the analysis. It can be difficult to find isolated lines in congested atmospheric spectra. Allowing windows that contain multiple strong lines provides improved flexibility, making it easier to avoid gaps in the wavenumber coverage. For the current study, it also permits extending the analysis closer to the limits of the instrument wavenumber range, reducing the potential impact of extrapolating the derived wavenumber dependences for empirical parameters beyond the analysis range, a significant danger when using simple Taylor expansions like the ones in Eqs. (3), (5), and (7).

Table 2 lists the additional windows employed in the analysis, on top of the set of isolated lines presented in Table 1. Similar to the procedure for isolated lines, spectra were included in the averages for these windows only where the minimum transmittance in the window was less than 0.95 and the minimum transmittance in the infinite resolution spectrum was greater than 0.1.

During the fitting process, calculations begin by generating the “residual modulation function” at the given wavenumber, employing the empirical representation described previously. The true modulation function is then calculated by multiplying through by the sinc function describing the field-of-view effect at that wavenumber.

Normally, the ILS would then be calculated from the Fourier transform of the true modulation function, and the signal would subsequently be calculated by convolving the ILS with the calculated infinite resolution spectrum. For this study, however, we instead calculate what we previously referred to as the “modified

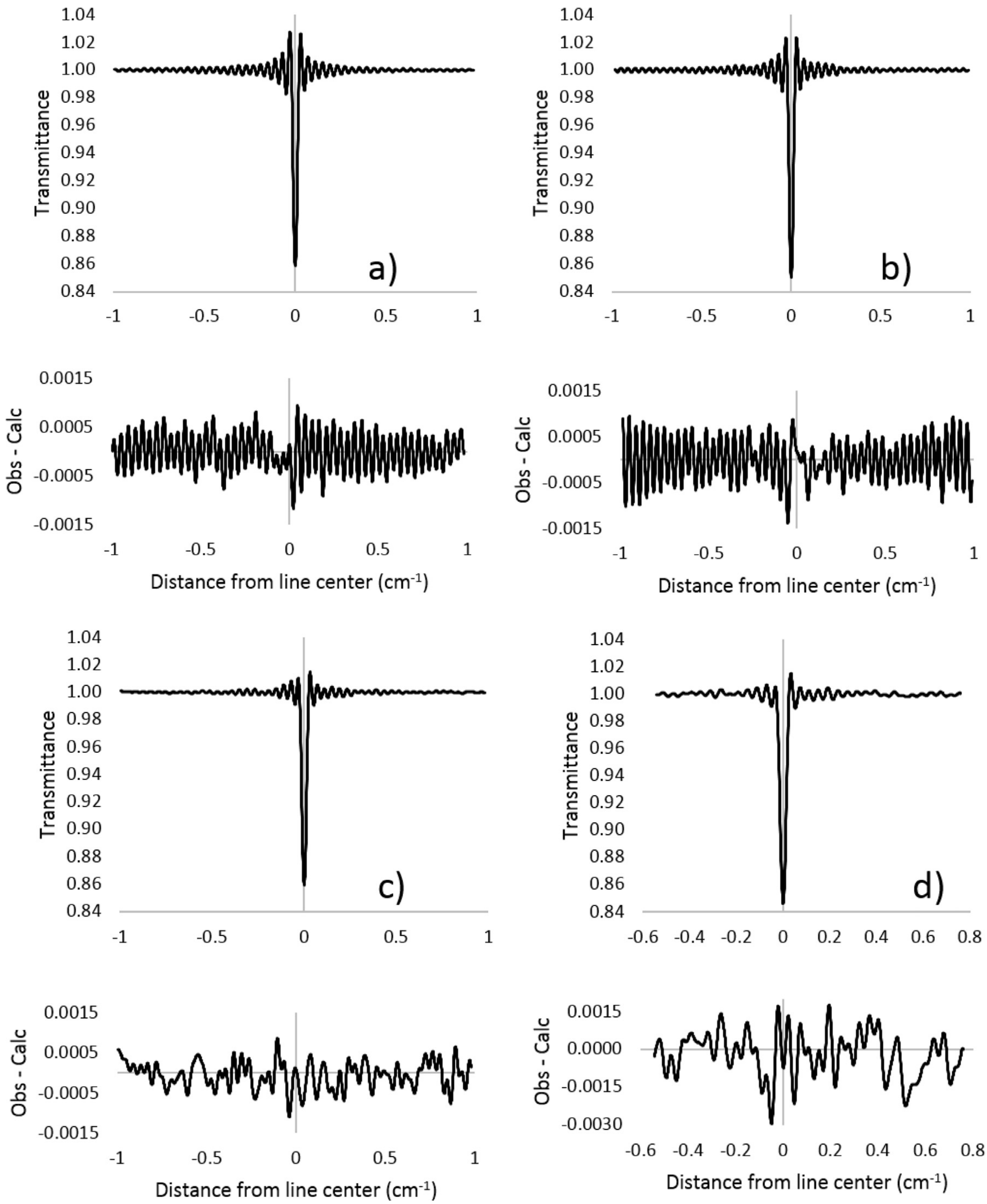

Fig. 7. The transmittances and fitting residuals for selected isolated lines: (a) 1487 cm^{-1}, (b) 2337 cm^{-1}, (c) 3254 cm^{-1}, and (d) 3807 cm^{-1}.

Table 2
Additional (multi-line) windows employed in the determination of the ACE-FTS ILS.

Window center (cm^{-1})	Window width (cm^{-1})	Molecules	Altitude range (km)
803.15	1.70	CO_2, O_3, H_2O	30–50
1025.70	2.00	O_3, CO_2	50–72
1121.33	2.82	O_3, H_2O	35–60
1187.03	1.45	H_2O, O_3, N_2O	35–60
1255.00	2.00	CH_4, N_2O, CO_2	35–65
1967.00	2.00	H_2O, CO_2	50–75
2618.12	1.44	CH_4, CO_2	30–45
2822.20	1.85	HCl, CH_4	35–55
4138.95	1.50	H_2O, CH_4	27–47

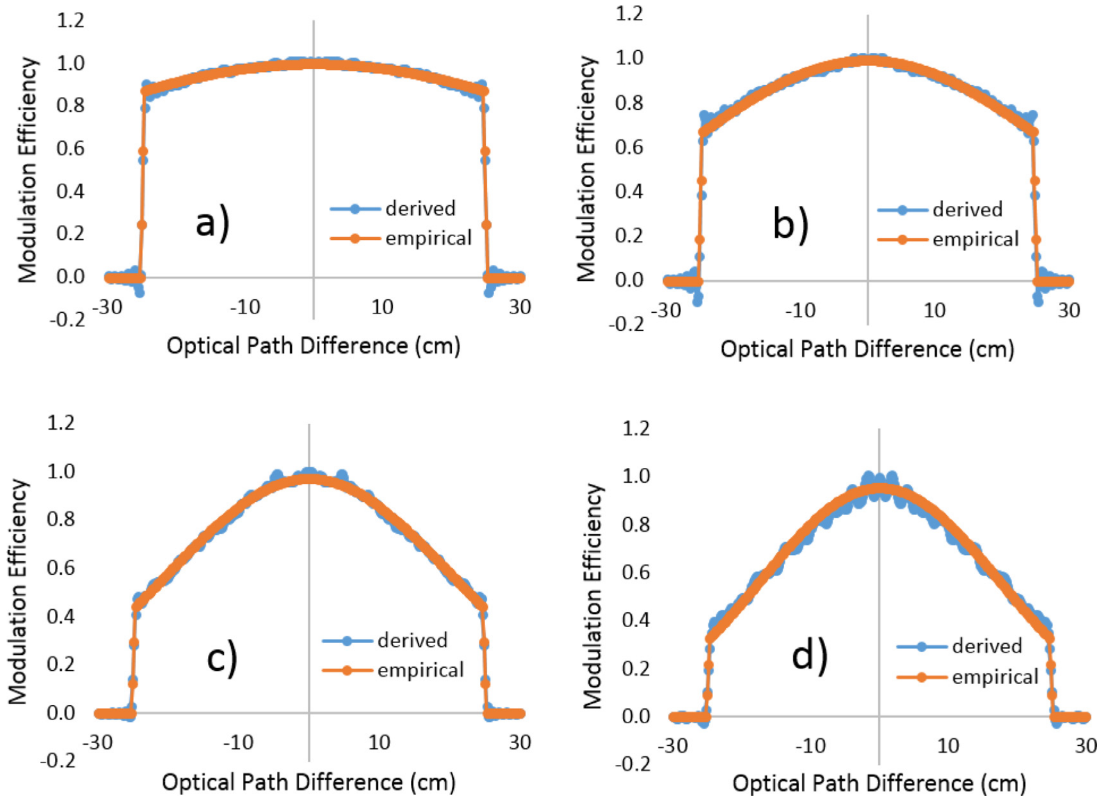

Fig. 8. Comparison of modulation function amplitudes. The "derived" curve (in blue) is the real component of the Fourier transform of the average measured line. The "empirical" curve (in orange) is calculated from the empirical function, determined from the fitting of averaged transmittance spectra. Results are shown for four selected lines: (a) 1487 cm^{-1}, (b) 2337 cm^{-1}, (c) 3254 cm^{-1}, and (d) 3807 cm^{-1}.

modulation function," multiplying the true modulation function by the Fourier transform of an isolated line in the infinite resolution spectrum. The transmittance signal is then calculated as 1.0 minus a scaling factor times the Fourier transform of the modified modulation function. The scaling factor is treated as a fitting parameter in the least-squares analysis. In windows containing multiple lines, each line is treated independently, fitting for the position and an intensity scaling factor for each individual line. Again, it is important to remember that the line shape determined by this approach corresponds to the mirror image of the ILS, and so the resulting phase must be inverted (multiplied by -1).

The analysis was performed in the above manner in order to simplify the treatment of windows containing multiple lines. In principle, one could calculate the spectrum through more conventional means, convolving the ILS with the calculated infinite resolution spectrum. In such a case, if convolution with the infinite resolution spectrum were included in the calculation during the fitting, the phase would not be inverted (the mirroring inherent in the convolution process would implicitly be taken into account, whereas it is not in the procedure described here).

To be rigorous, the calculated spectra in the windows employed here would need to account for isotopic fractionation of subsidiary isotopologues relative to the main isotopologue [31] and might require small adjustments to the line positions and intensities from the line list to minimize fitting residuals. Keep in mind, however, that we are not analyzing gas cell spectra. The data here are averaged spectra from thousands of occultations. Each individual measurement has its own unique geometry, and a forward model calculation for the measurement involves integration along the path traveled by a solar ray as it transits the atmosphere, with ranges of pressure and temperature encountered along the path. Rather than fit for spectroscopic parameters (line position and intensity) where each iteration in the least squares analysis would involve determining the average spectrum from thousands of forward model calculations, with a different set of atmospheric conditions and geometry for each calculation, we instead construct the spectrum from a set of individual lines, positioning each line in wavenumber and scaling each line in amplitude such that the constructed spectrum reproduces the measurement. This approach achieves residuals at the same level one could obtain from fitting the spectroscopic parameters while significantly reducing the complexity of the analysis.

In order to simplify the calculations, a common infinite resolution spectral line shape was employed for every line of a particular molecule in a given window, calculated from the strongest line for the molecule contained within the window. To be rigorous, one could calculate a different modified modulation function for each individual line (using their line shape in the calculated infinite resolution spectrum), but at the pressures associated with the measurements in the current study, where conditions were at the Doppler limit, assuming a common line shape for all the lines from a particular molecule in the given window provided sufficient accuracy.

All windows from Tables 1 and 2 were fitted simultaneously, determining the 6 parameters from the empirical representation for the modulation function amplitude plus the 8 parameters from the modulation function phase. The baseline phase (from Fig. 5a) was not adjusted but remained fixed to the average of the calculated phases for isolated lines at lower wavenumbers (between 1300 and 1800 cm^{-1}). Scaling factors for every analyzed line were also fitted, along with the positions of the various lines in windows containing multiple lines, but these last two categories of parameters are not intrinsic to the ILS and are therefore not reported.

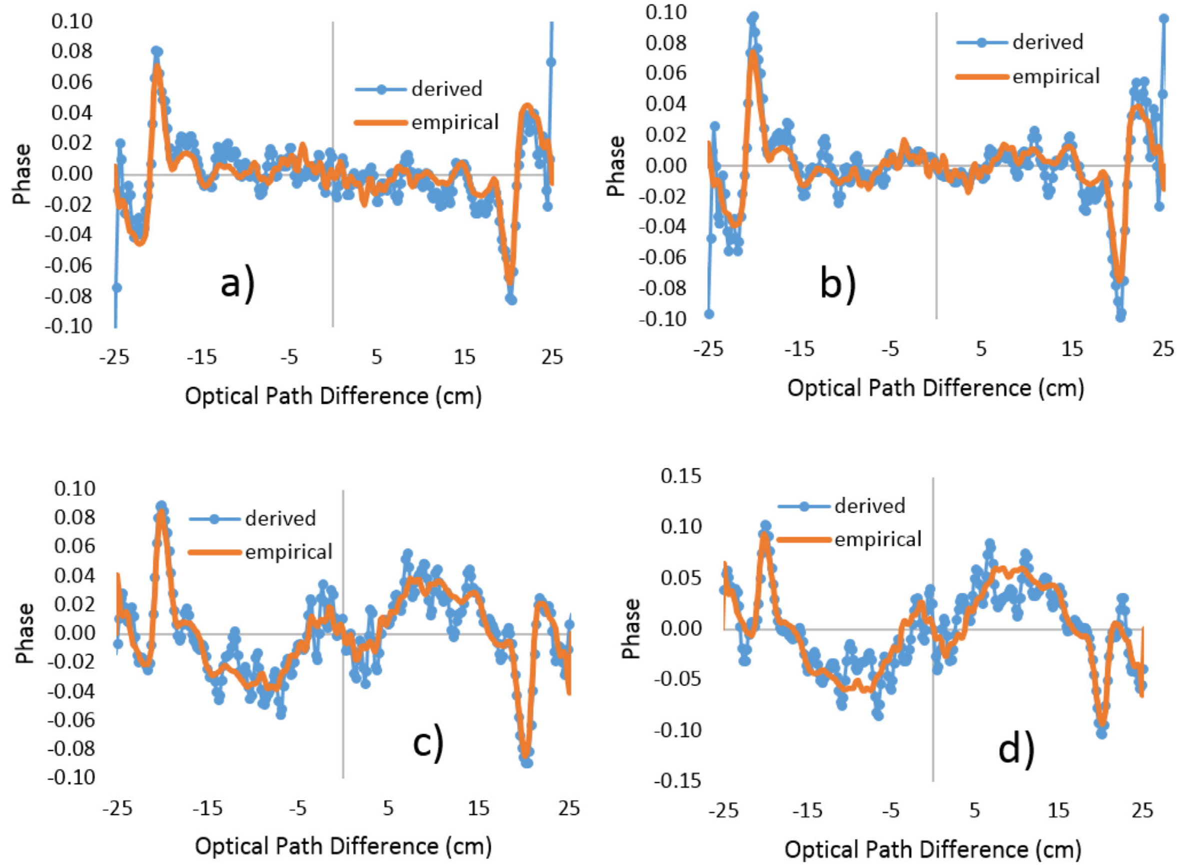

Fig. 9. Comparison of modulation function phases. The "derived" curve (in blue) is the imaginary component of the Fourier transform of the average measured line. The "empirical" curve (in orange) is calculated from the empirical function, determined from the fitting of averaged transmittance spectra. Results are shown for four selected lines: (a) 1487 cm^{-1}, (b) 2337 cm^{-1}, (c) 3254 cm^{-1}, and (d) 3807 cm^{-1}.

Table 3
Empirical parameters for the ACE-FTS ILS.

Amplitude	Inverse of phase
Cliff edge = 24.64748 cm	a_{D0} = −8.034849e-2
Cliff slope = 2.033965	a_{D1} = −9.02245e-4
a_{G0} = 33.004634	a_{D2} = 6.381116e-7
a_{G1} = −1.737389e-2	b_D = 3.1645974
a_{G2} = 1.108927456e-5	a_{S0} = −2.473988e-3
a_{G3} = −3.4418703e-9	a_{S1} = 1.22786e-5
	a_{S2} = −1.038028e-8
	b_S = 0.17416585

5. Results

The empirical parameters determined for the ACE-FTS ILS are presented in Table 3. Plots of the wavenumber variations for $a_G(\tilde{\nu})$, $a_D(\tilde{\nu})$, and $a_S(\tilde{\nu})$ are provided in Fig. 6, with the wavenumbers of isolated lines and multi-line windows employed in the analysis indicated. As suggested by the plots, care was taken to avoid significant gaps in the wavenumber coverage of the instrument.

The random fitting errors for individual parameters in Table 3 are typically smaller than ten percent (a reasonable fitting error was one of the criteria used to determine whether to keep a particular parameter in the final function). However, these parameters are highly correlated, and so excess significant digits are retained in all parameters to ensure no rounding errors in the calculated function.

This instrumental line shape represents a significant improvement over the one employed in ACE-FTS version 3 processing. The chi-squared goodness of fit parameter is generally 5 to 10 percent smaller with the new ILS, depending on the molecule being analyzed.

Fig. 7 shows the average transmittance and fitting residuals (observed – calculated) for four selected isolated lines. The increasing asymmetry with increasing wavenumber is evident in the strong skew in the sidelobes for lines at higher wavenumber. Contributions to the residuals from neighboring lines (not included in the calculations) are evident at lower wavenumbers in Fig. 7, where the damping of sidelobes as you move away from line center is smaller. If the gas sample features lines that are too close together, it may be necessary to take neighboring lines into account, but such effects were neglected in the current study.

In the residual plots in Fig. 7, there is perhaps some indication of minor difficulties characterizing the first sidelobes, possibly stemming from the assumption of a fixed baseline contribution to the phase, when there is likely a small wavenumber variation inherent in the structure near MOPD. Note, however, that the residuals in Fig. 7 are well below the noise level for a single ACE-FTS measurement at the given wavenumber. Overall, fitting residuals were typically more than a factor of 5 smaller than the ACE-FTS noise level, suggesting that any remaining deficiencies in the ILS characterization should not have a significant impact on individual retrievals from ACE-FTS spectra.

Although we are fitting the original transmittances rather than the derived modulation function amplitude and phase, the modulation function is calculated as a step in the analysis. We can therefore compare the calculated modulation function amplitude and phase to the derived curves from isolated lines, as a check for

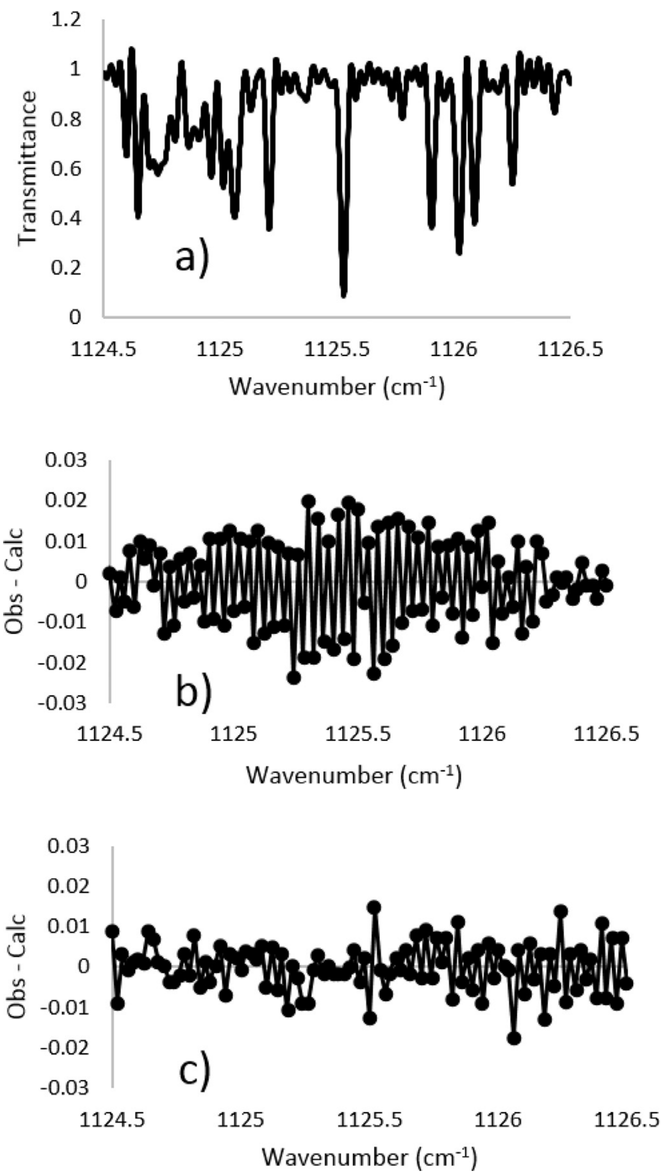

Fig. 10. (a) A spectral window in a dense O_3 region for a measurement near 31 km in occultation sr10063, interpolated in wavenumber. (b) Residuals (observed - calculated) in the window using the ACE-FTS version 3 ILS. (c) Residuals with the new version 4 ILS.

internal consistency. Fig. 8 shows the agreement of the amplitudes for a selected set of lines, while Fig. 9 makes the comparisons for the modulation function phase.

The agreement in Figs. 8 and 9 are reasonably good, as they should be if the empirical representation was properly chosen. In Fig. 9, for the lower wavenumber lines, spikes in the derived phase near MOPD appear to arise from sidelobes from neighboring lines "leaking" into the window, as previously mentioned.

Perhaps the best gauge of the improvement in the ILS can be observed from fitting residuals in spectral regions containing many O_3 lines. With the ACE-FTS version 3 ILS, there would often be bursts of oscillatory features in the residuals under such conditions, as can be seen in Fig. 10b. With so many overlapping lines, small errors in the ILS can lead to a relatively large accumulation of enhanced residuals. This can impact the results for weak absorbers (like HCFC-141b and HCFC-142b) that have spectral features in the midst of dense O_3 spectral regions, potentially introducing systematic errors in retrieval results for the weak absorber. Note that the residual (observed - calculated) plots in Fig. 10b and c are on the native (0.02 cm^{-1}) grid, the grid upon which the least-squares fitting is performed in the retrievals, while the spectrum in Fig. 10a is provided on a finer wavenumber grid, Fourier interpolated by a factor of 16 to better see details.

With the ACE-FTS version 4 ILS, residuals in the vicinity of cluttered O_3 regions are significantly reduced, as seen in Fig. 10c. This should improve the quality of version 4 retrieval results for weak absorbers subject to a large number of overlapping lines. It will also improve the prospects of retrieving additional weakly-absorbing HFCs and CFCs that occur in the 1100 to 1150 cm^{-1} range, which is a region containing a high density of O_3 spectral features.

6. Conclusions

A procedure has been described to generate a highly accurate representation of a Fourier transform spectrometer instrumental line shape, applicable even for situations involving significant structure. Using isolated spectral features measured at low pressure (ideally averaged to reduce noise effects), the modulation function amplitude and phase can be directly calculated if the shape of the line in the infinite resolution spectrum is reasonably well known. From a set of lines covering a wide range of wavenumbers, the ideal form for an empirical representation and the wavenumber dependences for any parameters in that representation can then be readily deduced, with no need to guess at a form. Fitting a set of lines spanning as much of the instrument wavenumber range as possible, values for the parameters in the empirical representation can be determined, and the ILS can thus be accurately calculated at any wavenumber.

This approach has been applied to characterize the ILS of the ACE-FTS instrument on board the SCISAT satellite. This will feed into improved retrievals for the upcoming version 4 processing of the full mission data set for the instrument. The resulting reduction in residuals may also help with generating retrievals for additional weak absorbers for future processing versions.

Based on the ACE-FTS ILS analysis, there is some question of the validity of employing an effective field of view to account for self-apodization effects. The shape of the residual self-apodization was inconsistent with a broadening of the sinc function used for the field of view effect, but a Gaussian apodization function reproduced the shape quite well.

Acknowledgment

Funding was provided by the Canadian Space Agency.

References

[1] Davis SP, Abrams MC, Brault JW. Fourier transform spectroscopy. San Diego: Academic Press; 2001.
[2] Gunson MR, Abbas MM, Abrams MC, Allen M, Brown LR, Brown TL, et al. The atmospheric trace molecule spectroscopy (ATMOS) experiment: deployment on the ATLAS space shuttle missions. Geophys Res Lett 1996;23:2333–6.
[3] Suzuki M, Matsuzaki A, Ishigaki T, Kimura N, Yokota T, Sasano Y. ILAS, the improved atmospheric spectrometer, on the advanced earth observing satellite. IEICE Trans Commun 1995;E78-B:1560–1570.
[4] Fischer H, Oelhaf H. Remote sensing of vertical profiles of atmospheric trace constituents with MIPAS limb-emission spectrometers. Appl Opt 1996;35:2787–96.
[5] Beer R, Glavich TA, Rider DM. Tropospheric emission spectrometer for the earth observing system's aura satellite. Appl Opt 2001;40:2356–67.
[6] Bernath PF, McElroy CT, Abrams MC, Boone CD, Butler M, Camy-Peyret C, et al. Atmospheric Chemistry Experiment (ACE): mission overview. Geophys Res Lett 2005;32:L15S01. doi:10.1029/2005GL022386.

[7] Kuze A, Suto H, Nakajima M, Hamazaki T. Thermal and near infrared sensor for carbon observation Fourier-transform spectrometer on the greenhouse gases observing satellite for greenhouse gases monitoring. Appl Opt 2009;48:6716–33.

[8] Clerbaux C, Boynard A, Clarisse L, George M, Hadji-Lazaro J, Herbin H, et al. Monitoring of atmospheric composition using the thermal infrared IASI/MetOp sounder. Atmos Chem Phys 2009;9:6041–54.

[9] Toon GC. The JPL MkIV Interferometer. Opt Photon News 1991;2:19–21. doi:10.1364/OPN.2.10.000019.

[10] Fu D, Walker KA, Sung K, Boone CD, Soucy M-A, Bernath PF. The portable atmospheric research interferometric spectrometer for the infrared, PARIS-IR. J Quant Spectrosc Radiat Transf 2007;103:362–70.

[11] De Mazière M, Thompson AM, Kurylo MJ, Wild JD, Bernhard G, Blumenstock T, et al. The network for the detection of atmospheric composition change (NDACC): history, status and perspectives. Atmos Chem Phys 2018;18:4935–64.

[12] Wunch D, Toon GC, Blavier J-FL, Washenfelder RA, Notholt J, Connor BJ, et al. The total carbon column observing network. Philos Trans R Soc A: Math Phys Eng Sci 2011;369:2087–112.

[13] Loos J, Birk M, Wagner G. Measurement of positions, intensities and self--broadening line shape parameters of H_2O lines in the spectral ranges 1850–2280 cm^{-1} and 2390–4000 cm^{-1}. J Quant Spectrosc Radiat Transf 2017;203:119–32.

[14] Harrison JJ. New and improved infrared absorption cross sections for dichlorodifluoromethane (CFC-12). Atmos Meas Technol 2015;8:3197–207.

[15] Norton H, Beer R. New apodizing functions for Fourier spectrometry. J Opt Soc Am 1976;66:259–64.

[16] Benner DC, Devi VM, Sung K, Brown LR, Miller CE, Payne VH, et al. Line parameters including temperature dependences of air- and self-broadened line shapes of $^{12}C^{16}O_2$: 2.06-μm region. J Mol Spectrosc 2016;326:21–47.

[17] Boone CD, Walker KA, Bernath PF. Version 3 retrievals for the atmospheric chemistry experiment Fourier transform spectrometer (ACE-FTS). In: Bernath PF, editor. The atmospheric chemistry experiment ACE at 10: a solar occultation anthology. Virginia: A Deepak Publishing; 2013. p. 103–27.

[18] Hase F, Blumenstock T, Paton-Walsh C. Analysis of the instrumental line shape of high-resolution Fourier transform IR spectrometers with gas cell measurements and new retrieval software. Appl Opt 1999;38:3417–22.

[19] Bernath PF. The atmospheric chemistry experiment (ACE). J Quant Spectrosc Radiat Transf 2017;186:3–16.

[20] Bujis HL, Soucy M-A, Lachance RL. ACE-FTS hardware and level 1 processing. In: Bernath PF, editor. The atmospheric chemistry experiment ACE at 10: a solar occultation anthology. Virginia: A. Deepak Publishing; 2013. p. 53–80.

[21] Boone CD, Nassar R, Walker KA, Rochon Y, McLeod SD, Rinsland CP, Bernath PF. Retrievals for the atmospheric chemistry experiment Fourier-transform spectrometer. Appl Opt 2005;44(33):7218–31.

[22] Zasetsky AY, Gilbert K, Galkina I, McLeod S, Sloan JJ. Properties of polar stratospheric clouds obtained by combined ACE-FTS and ACE-Imager extinction measurements. Atmos Chem Phys Discuss 2007;7:13271–90.

[23] Petelina SV, Zasetsky AY. Temperature of mesospheric ice particles simultaneously retrieved from 850 cm^{-1} libration and 3200 cm^{-1} vibration band spectra measured by ACE-FTS. J Geophys Res: Atmos 2011;116:D03304.

[24] Doeringer D, Eldering A, Boone CD, Gonzalez Abad G, Bernath PF. Observation of sulfate aerosols and SO_2 from the Sarychev volcanic eruption using data from the atmospheric chemistry experiment (ACE). J Geophys Res Atmos 2012;117:D03203.

[25] Bernardo C, Griffith DWT. Fourier transform spectrometer instrument lineshape (ILS) retrieval by Fourier deconvolution. J Quant Spectrosc Radiat Transf 2017;95:141–50.

[26] Raspollini P, Ade P, Carli B, Ridolfi M. Correction of instrument line-shape distortions in Fourier transform spectroscopy. Appl Opt 1998;37(17):3697–3704.

[27] Bianchini G, Raspollini P. Characterisation of instrumental line shape distortions due to path difference dependent phase errors in a Fourier transform spectrometer. Infrared Phys Technol Appl Opt 2000;41:287–92.

[28] Edwards DP, López-Puertas M, López-Valverde MA. Non-local thermodynamic equilibrium studies of the 15-μm bands of CO_2 for atmospheric remote sensing. J Geophys Res 1993;98(D8) 14,955-14,977.

[29] Jacquemart D, Sung K, Coleman M, Crawford T, Brown LR, Mantz AW, Smith MAH. Measurements and modeling of $^{16}O^{12}C^{17}O$ spectroscopic parameters at 2 μm. J Quant Spectrosc Radiat Transf 2017;203:249–64.

[30] Ota Y, Imasu R. CO_2 retrieval using thermal infrared radiation observation by interferometric monitor for greenhouse gases (IMG) onboard advanced earth observing satellite (ADEOS). J Meteorol Soc Jpn 2016;94:471–90.

[31] Buzan EM, Beale CA, Boone CD, Bernath PF. Global stratospheric measurements of the isotopologues of methane from the atmospheric chemistry experiment Fourier transform spectrometer. Atmos Meas Tech 2016;9:1095–111.